Analysis of the three dimensional focal positioning capability of adaptive optic elements

P. S. Salter,[1] Z. Iqbal,[1] and M. J. Booth[1,2]

[1]*Department of Engineering Science, University of Oxford,Parks Road, Oxford, OX1 3PJ, UK*

[2]*Centre for Neural Circuits and Behaviour, University of Oxford, Mansfield Road, Oxford OX1 3SR, UK*

(Dated: March 14, 2013)

Abstract

There are many situations where adaptive optic elements are useful for beam steering. When the beam is passed through a lens the resulting focus may be scanned within a three dimensional volume. In this article, we introduce expressions to describe the maximum distance to which a focus may be steered using a deformable mirror with a continuous phase distribution, limited either in its gradient or amplitude. Additionally for liquid crystal spatial light modulators (SLMs), an analytic approach is developed to describe the intensity reduction of a steered focus due to phase wrapping and pixellation. By calculating the total area on the SLM taken up by phase wrapping, we can estimate the proportion of light that is not directed to the focus. Thus, we derive an expression for the 3D volume within which we may steer a focus given a permissible reduction in intensity. The results compare favourably with experiment.

Published in the International Journal of Optomechatronics, Volume 7, Feb 2013, 1-14. (DOI:10.1080/15599612.2012.758791)

I. INTRODUCTION

An adaptive optic element (AOE) offers the capability to alter the phase of an incident wavefront across a laser beam [1]. Common examples of AOEs are deformable mirror devices or liquid crystal spatial light modulators (SLMs). There are many diverse applications for AOEs, including adaptive correction of aberrations in the laser beam path [2, 3]; the spectral control of ultrashort laser pulses [4]; or the generation of focal arrays for either optical tweezing [5, 6] or laser microfabrication [7, 8]. An alternative application for such an adaptive element is non-mechanical laser beam steering [9], which holds technological interest for devices such as optical interconnects [10] and video projection systems [11].

When the beam is transformed by a lens, the beam steering capacities of the AOE are manifested as a spatial scanning of the associated focus. A linear phase gradient shifts the focus laterally (within the focal plane), while imposing a phase with appropriate curvature corresponds to an axial shift or refocussing. These capabilities are extremely useful for optical tweezers in applications such as optical clamping [12]. There have been various theoretical and experimental studies into the focal positioning limits of AOEs, particularly using liquid crystal SLMs and concentrating on the reduction in focal intensity with distance from the natural focus [13–17]. Much of the theoretical work involves complex modelling of the liquid crystal alignment field in the SLM and calculation of light propagation through the resultant structure. In this work, we develop simple analytic expressions to describe the 3D volume accessible for focal positioning using different AOEs. The analysis is such that it may be easily extended for more complex phase patterns, such as those where spatially dependent aberration compensation is included or for the generation of multiple foci.

II. ACCESSIBLE STEERING VOLUME USING CONTINUOUS PHASE PATTERNS

A collimated beam of light is incident on a phase-only AOE, which is situated in the back-focal plane of a lens with focal length f. The AOE defines the effective pupil aperture of the lens, and is assumed to have a radius of one. Coordinates in the pupil plane are (r, θ) and it is also assumed the beam has uniform amplitude over the pupil. The lens transforms the beam to a diffraction-limited focus, while the AOE may alter the phase profile across the beam in order to shift the focus in the Fourier space, as indicated in Figure 1. The phase function the AOE needs to apply to the wavefront to displace the focus to a point (ρ, ξ, z) in image space is [18]:

$$\Psi(r,\theta) = k\left[-\rho r \sin\alpha\cos(\theta-\xi) + z\sqrt{1-r^2\sin^2\alpha}\right] \tag{1}$$

where $k = \frac{2\pi}{\lambda}$ and α is the focusing angle of the lens used. Cylindrical coordinates are used at the focus ($x = \rho\cos\xi$ and $y = \rho\sin\xi$). Note that the defocus function is defined as spherical rather than parabolic, as appropriate for microscope objectives designed to fulfill the sine condition. This is especially important for objectives with high numerical apertures (NA).

Our aim is to determine how far we can usefully steer the focus given the limitations of the AOE. Initially, we simply consider the case where the AOE can be used to display a continuous phase pattern (i.e. there is no phase wrapping). This is true for AOEs such as membrane deformable mirrors. The operating range of such an AOE may be limited in

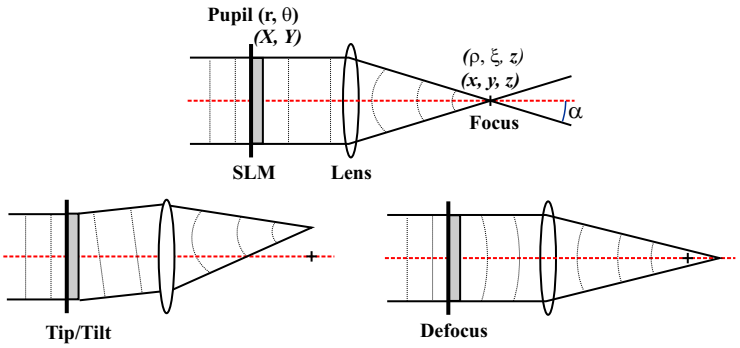

FIG. 1: The AOE is used to alter the phase of incident wavefronts to displace the focal spot. Tip/tilt applied to the AOE shifts the focus laterally within the focal plane, while defocus translates along the optic axis.

two ways: i) the mechanics of the AOE may limit the maximum phase gradient between actuators or ii) the AOE may be limited to a maximum phase modulation. We consider each of these scenarios below.

A. Limited phase gradient

We denote the maximum possible gradient in a phase pattern that can be reliably reproduced by the AOE as g_{max}:

$$|\nabla\Psi| \leq g_{max} \tag{2}$$

Referring to Equation 1, our expression becomes:

$$|\nabla\Psi|^2 \leq g_{max}^2 \tag{3}$$

$$\left|\left(-\rho k \sin\alpha\cos(\theta-\xi) - \frac{zkr\sin^2\alpha}{\sqrt{1-r^2\sin^2\alpha}}\right)\underline{\hat{e_r}} + k\rho\sin\alpha\sin(\theta-\xi)\underline{\hat{e_\theta}}\right|^2 \leq g_{max}^2 \tag{4}$$

$$\rho^2k^2\sin^2\alpha + \frac{z^2k^2r^2\sin^4\alpha}{1-r^2\sin^2\alpha} + \frac{2zr\rho k^2\sin^3\alpha\cos(\theta-\xi)}{\sqrt{1-r^2\sin^2\alpha}} \leq g_{max}^2 \tag{5}$$

where we have denoted unit vectors in the radial and azimuthal direction as $\underline{\hat{e_r}}$ and $\underline{\hat{e_\theta}}$ respectively. Simplifying and taking into account that the phase gradient is always maximum when $r = 1$, the resultant maximum values of ρ and z for which the AOE can displace the focus follow the relationship:

$$\rho_{max} + z_{max}\tan\alpha = \frac{g_{max}}{k\sin\alpha} \tag{6}$$

Equation 6 denotes the volume that can be accessed by the focal spot given the AOE can apply a maximum possible phase gradient. The shape is two cones joined end to end at the plane $z = 0$ with a radius $g_{max}/k\sin\alpha$ and extending to $\pm z$ a distance $g_{max}/k\sin\alpha\tan\alpha$, as shown in Figure 2. The angle the surface of the cone makes with the optical axis is the same as the focusing angle of the lens, α.

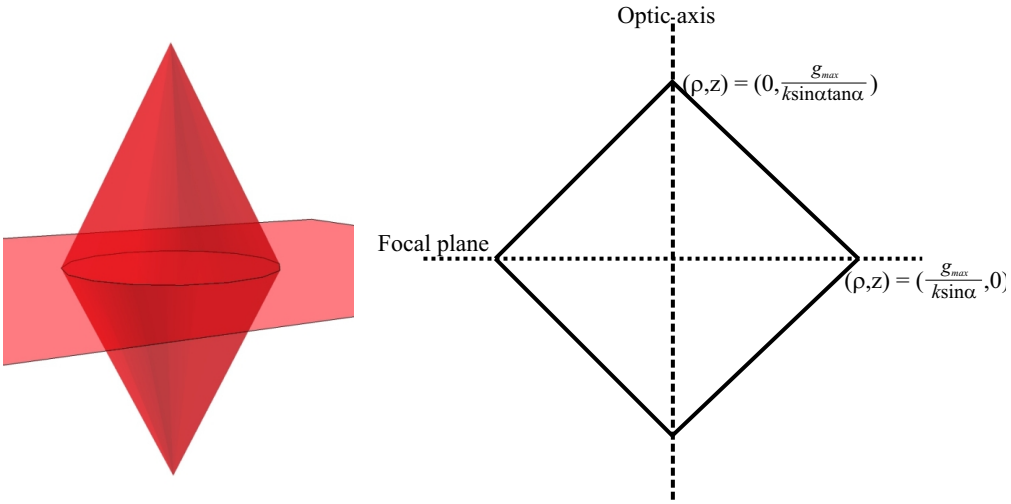

FIG. 2: The volume accessible to focal steering for the case where the adaptive element is a continuous phase shape limited by a maximum phase gradient g_{max}.

B. Limited phase range

The AOE may alternatively be limited in focal steering by a maximum achievable phase range. Again, this is of particular relevance to continuous phase patterns displayed on deformable mirrors with limited actuator displacement. We denote the difference between the maximum and minimum possible phase values as $\Delta\psi_{\mathrm{M}} = \psi_{max} - \psi_{min}$, and set about determining the volume accessible to focal steering. If the focus is simply translated within the focal plane ($z = 0$), the maximum and minimum phase values will occur at pupil coordinates $(r, \theta) = (1, \xi + \pi)$ and $(1, \xi)$. Thus from Equation 1 we can write down an expression for ρ_{max} in terms of $\Delta\psi_{\mathrm{M}}$:

$$\frac{\Delta\psi_{\mathrm{M}}}{k} = 2\rho_{max}\sin\alpha \tag{7}$$

In the case where $z \neq 0$, to identify the pupil coordinates (r', θ') of an extremum we need to set the derivative $\nabla\Psi$ (given in Equation 5) equal to zero. The opposite extreme value of the phase within the pupil is found at the pupil edge ($r = 1$) and will be at an azimuthal coordinate differing by π radians ($\theta' + \pi$). After some simplification, an expression for ρ_{max} and z_{max} is found in terms of the maximum phase range $\Delta\psi_{\mathrm{M}}$:

$$\frac{\Delta\psi_{\mathrm{M}}}{k} = \sqrt{\rho_{max}^2 + z_{max}^2} + \rho_{max}\sin\alpha - z_{max}\cos\alpha \tag{8}$$

The transition between Equations 7 and 8 depends on the focussing angle α and can be found by setting them equal:

$$\rho_{max}\cos\alpha = z_{max}\sin\alpha \tag{9}$$

Thus the volume accessible for focal positioning in the case of a maximum AOE phase range $\Delta\psi_{\mathrm{M}}$ is represented by Equations 7 and 8, with the transition defined by Equation 9.

The volume is sketched in Figure 3. A cylinder of radius $\Delta\psi_{\rm M}/2k\sin\alpha$ extends to a maximum z shift of $\Delta\psi_{\rm M}/2k\sin\alpha\tan\alpha$. For larger values of z, the maximum range is a more complex function of ρ and z, shown by the rounded cone form in Figure 3.

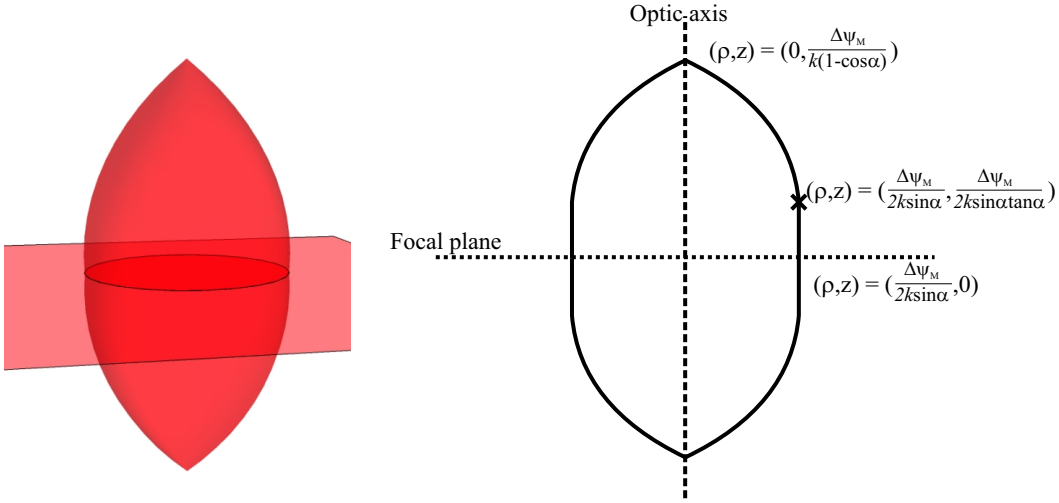

FIG. 3: The volume accessible to focal steering for the case where the adaptive element is a continuous phase shape limited by a maximum phase amplitude $\Delta\psi_{\rm M} = |\psi_{max} - \psi_{min}|$.

III. VOLUME ACCESSIBLE TO WRAPPED PHASE PATTERNS

The liquid crystal SLMs typically used in experiment are incapable of displaying large amplitude continuous phase patterns, as considered in the previous section, since the maximum range is often 2π. However, since the SLM has a large number of pixels, wherever the phase pattern reaches a value of 2π it may be wrapped back to zero, as shown in Figure 4. Since the liquid crystal basis for the SLM is a continuous medium, the $2\pi \rightarrow 0$ phase change (the "flyback region") has a finite width designated t. In the "flyback region" the SLM does not display the required phase pattern and the light incident on this area of the SLM is not directed to the desired location. Consequently, the intensity of the focal spot is reduced, with light being redistributed to the zero and higher orders.

To determine the reduction in intensity at the focus, the total area of the pupil occupied by phase wraps on the SLM needs to be calculated. The reduction of area of the pupil due to phase wrapping should be directly proportional to the intensity at the focus. Initially, for illustration of the method we consider solely the effects of defocus (positioning the focal spot at a point $x = y = 0, z \neq 0$) such that the phase wraps are circular. It is useful to express the phase at a point (r, θ) by:

$$\Psi(r,\theta) = \int_0^r \frac{\partial \Psi}{\partial r} dr \tag{10}$$

The number of phase wraps between the origin and this point is the same as the number of times that the phase function has the value $2n\pi$ radians, where n is an integer. The expected

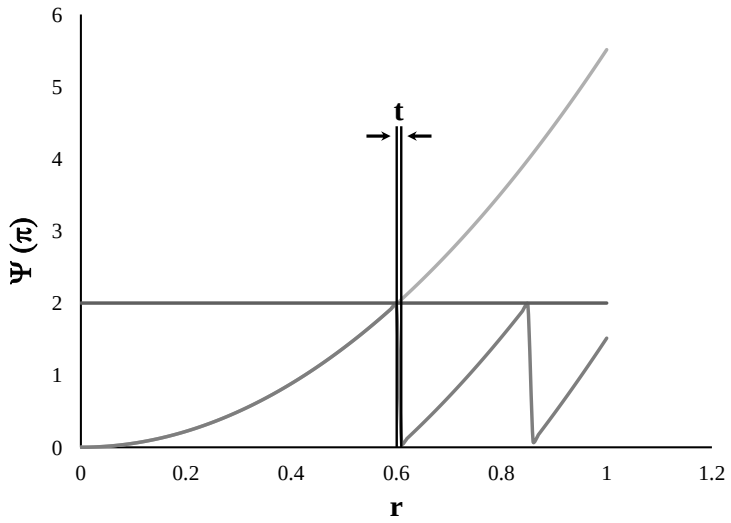

FIG. 4: The phase wrapping properties of the SLM lead to an area of the pupil plane (thickness t per wrap) that does not display the required phase pattern, from which light is not directed to the desired focus.

number of phase wraps encountered up to this point is therefore found by dividing $\Psi(r,\theta)$ by 2π. Each of these circular phase wraps will occupy an area $rt\,d\theta$. Thus the area of the pupil occupied by phase wraps can be calculated as the sum of these areas. In a continuous approximation, this area A' can be expressed as:

$$A' = \int_0^1 \int_0^{2\pi} \frac{\partial \Psi}{\partial r} \frac{rt}{2\pi} dr d\theta \tag{11}$$

These arguments can be extended to a more general form of phase function to give the effective area of the pupil as:

$$A_{eff} = \pi - \int_0^1 \int_0^{2\pi} \frac{t}{2\pi} \left|\nabla \Psi\right| r dr d\theta \tag{12}$$

The modulus of $|\nabla\Psi|$ is required for the extension of the work to more complicated phase patterns where there may be both large positive and negative gradients in Ψ across the pupil. There is an additional caveat: the phase variation should be large in magnitude , hence exhibiting many phase wraps, for the integral calculation to be valid. For example, if the phase oscillates between $\frac{3\pi}{2}$ and $\frac{\pi}{2}$ across the pupil, Equation 12 would give a reduced effective area although there are no phase wraps. It is estimated that there need to be at least ~ 5 phase wraps across the pupil for the expression to become accurate.

From Equation 5, we have an expression for $|\nabla\Psi|$:

$$|\nabla\Psi| = \sqrt{\rho^2 k^2 \sin^2\alpha + \frac{z^2 k^2 r^2 \sin^4\alpha}{1 - r^2\sin^2\alpha} + \frac{2zr\rho k^2 \sin^3\alpha \cos(\theta - \xi)}{\sqrt{1 - r^2\sin^2\alpha}}} \tag{13}$$

Simplifying and denoting $r\sin\alpha = R$:

$$|\nabla\Psi| \;=\; \frac{k\sin\alpha}{\sqrt{1-R^2}} \left(\rho^2(1-R^2) + z^2R^2 + 2z\rho R\cos(\theta-\xi)\sqrt{1-R^2}\right)^{\frac{1}{2}} \tag{14}$$

$$= \frac{k\sin\alpha}{\sqrt{1-R^2}}\left(\rho^2(1-R^2)+z^2R^2\right)^{\frac{1}{2}}\left(1+\frac{2z\rho R\cos(\theta-\xi)\sqrt{1-R^2}}{\rho^2(1-R^2)+z^2R^2}\right)^{\frac{1}{2}} \quad (15)$$

To simplify further, it would be useful to eliminate the second bracket in Equation 15. A binomial expansion of that term gives:

$$1+\frac{1}{2}\frac{2z\rho R\cos(\theta-\xi)\sqrt{1-R^2}}{\rho^2(1-R^2)+z^2R^2}-\frac{1}{8}\left(\frac{2z\rho R\cos(\theta-\xi)\sqrt{1-R^2}}{\rho^2(1-R^2)+z^2R^2}\right)^2+\ldots \quad (16)$$

In order to eliminate this term in Equation 15, we require that the first and higher order terms are negligible. Since the ultimate goal is to integrate Equation 15 over the pupil, the cosine will be integrated with respect to θ from $0 \to 2\pi$. Any odd terms in the expansion in Equation 16 will hence integrate to zero. Even terms do not integrate to zero, but are given by [19]:

$$\int_0^{2\pi}\cos^n\theta d\theta = \frac{2\sqrt{\pi}\Gamma(\frac{n+1}{2})}{\Gamma(1+\frac{n}{2})} \quad (17)$$

Where $\Gamma(\ldots)$ represents the Euler Gamma function, and the value of the cosine integral decreases for higher order terms. After the integration over θ the expansion in Equation 16 becomes:

$$2\pi\left[1+-\frac{1}{16}\left(\frac{2z\rho R\sqrt{1-R^2}}{\rho^2(1-R^2)+z^2R^2}\right)^2+\ldots\right] \quad (18)$$

The most significant remaining term is the second order, which is found to have a maximum value of ~ 0.015 by varying R and z/ρ in the range $0 \leq R \leq 1$ and $-\infty \leq (z/\rho) \leq \infty$ respectively. Since all higher order terms in the expansion will be less than this, it is appropriate to approximate the Equation 16 as:

$$\left(1+\frac{2z\rho R\cos(\theta-\xi)\sqrt{1-R^2}}{\rho^2(1-R^2)+z^2R^2}\right)^{\frac{1}{2}} \cong 1 \quad (19)$$

and, hence, Equation 15 as:

$$|\nabla\Psi| \cong \frac{k\sin\alpha}{\sqrt{1-R^2}}\left(\rho^2(1-R^2)+z^2R^2\right)^{\frac{1}{2}} \quad (20)$$

To determine the effective area of the pupil lost to phase wrapping, Equation 20 needs to be integrated over the pupil:

$$\sigma = \frac{2\pi A'}{t} = \int_0^1\int_0^{2\pi}|\nabla\Psi|\,r dr d\theta = \frac{2\pi k}{\sin\alpha}\int_0^{\sin\alpha} R\left(\frac{\rho^2(1-R^2)+z^2R^2}{1-R^2}\right)^{\frac{1}{2}}dR \quad (21)$$

where we have introduced the quantity sigma, which is proportional to the area occupied by phase wraps. After some involved manipulation we arrive at the result:

$$\begin{aligned}\frac{\sin\alpha}{2\pi k}\sigma &= \frac{\rho}{2}-\frac{\sqrt{2}}{4}\cos\alpha\sqrt{z^2+\rho^2-(z^2-\rho^2)\cos 2\alpha} \quad (22)\\ &+\frac{z^2}{2\sqrt{z^2-\rho^2}}\arctan\left[\sqrt{z^2-\rho^2}\left(\frac{\sqrt{z^2+\rho^2-(z^2-\rho^2)\cos 2\alpha}-\rho\sqrt{1+\cos 2\alpha}}{(z^2-\rho^2)\sqrt{1+\cos 2\alpha}+\rho\sqrt{z^2+\rho^2-(z^2-\rho^2)\cos 2\alpha}}\right)\right]\end{aligned}$$

Equation 22 is plotted as a function of z and ρ in Figure 5 (a). It is proportional to the area of the pupil lost due to phase wrapping on the SLM as the focus is displaced to a point (ρ, ξ, z). As expected, this is azimuthally degenerate and as both ρ and z increase so does the area of the phase wraps. For comparison the result of the numerical integration of the full expression for $|\nabla\Psi|$ (Equation 15) is plotted in Figure 5 (b).

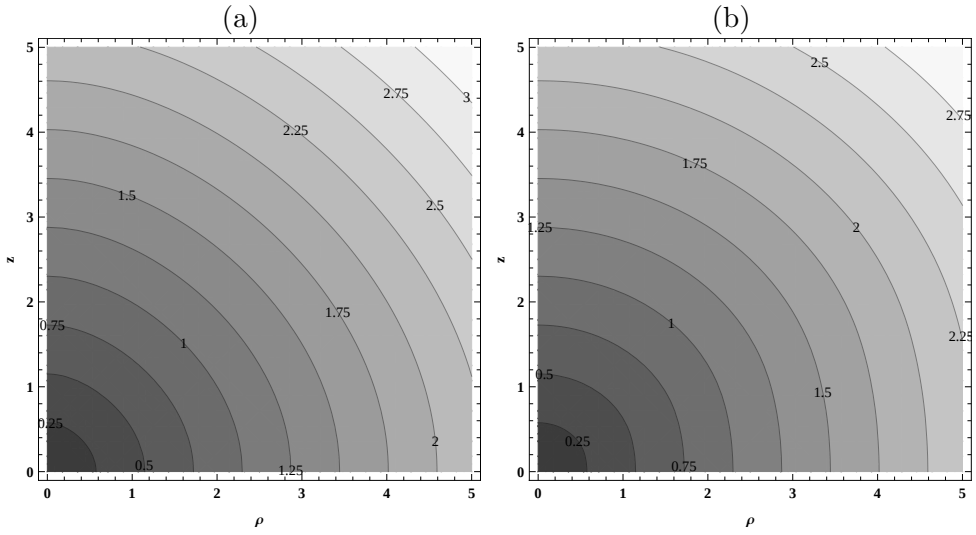

FIG. 5: (a) A plot of the result for $\frac{\sin\alpha}{2\pi k}\sigma$ from Equation 22 as a function of z and ρ and using a high numerical aperture $\sin\alpha = 1.4/1.5$, representing a high NA oil immersion objective lens.. (b) The same plot by the numerical integration of the full expression for $|\nabla\Psi|$ given in Equation 15.

The contours for both plots in Figure 5 are qualitatively similar in both shape and magnitude, and appear to have the approximate form of an ellipsoid. Hence, it would be useful if we could reduce Equation 22 to a simple elliptical form. As a rough approximation, we can simply take the intersection of Equation 22 with the ρ and z axes, which can then be used as the minor and major axes for an ellipse. When $z = 0$,

$$\frac{\sin\alpha}{2\pi k}\sigma = \frac{\rho}{2}\sin^2\alpha \tag{23}$$

and when $\rho = 0$:

$$\frac{\sin\alpha}{2\pi k}\sigma = \frac{z}{2}\left(\alpha - \frac{1}{2}\sin 2\alpha\right) \tag{24}$$

Thus we can construct an ellipse as:

$$\left(\frac{\sin\alpha}{2\pi k}\sigma\right)^2 = \frac{\rho^2}{4}\sin^4\alpha + \frac{z^2}{4}\left(\alpha - \frac{1}{2}\sin 2\alpha\right)^2 \tag{25}$$

This approximation actually provides a good fit to the calculated data. Indeed, the percentage error between the ellipse approximation in Equation 25 and the numerical integration of Equation 15 is consistently less than the equivalent error when compared to the approximate analytic expression in Equation 22. The maximum error as a function of ρ and z for the result of Equation 25 is less than 3% at high numerical aperture ($\sin\alpha = 1.4/1.5$). For decreasing numerical aperture, the error increases slightly to 6% when $\sin\alpha = 0.5$ before

dropping again to less than 2% for a low numerical aperture ($\sin\alpha = 0.1$). Overall, we can say that it is reasonable to use the much simplified form of Equation 25 to take into account of the effects of phase wrapping on the SLM. Thus, the full result for the effective area of the pupil (SLM) when steering the focus to a point (ρ, ξ, z) becomes:

$$A_{eff} = \pi - \frac{t}{2\pi}\sigma = \pi - \frac{tk}{\sin\alpha}\sqrt{\frac{\rho^2}{4}\sin^4\alpha + \frac{z^2}{4}\left(\alpha - \frac{1}{2}\sin 2\alpha\right)^2} \tag{26}$$

Since A_{eff} should correspond to the intensity of the focal spot, these results predict that the intensity should decrease linearly with distance from the zero order as the focus is translated along one of the axes. Figure 6 displays the volume accessible for focal translation using a LCSLM with phase wrapping, providing the focal intensity is at least 90% of that at the nominal focus. Regardless of the focussing numerical aperture, the volume is an oblate spheroid with dimensions always greater in the focal plane than along the optic axis.

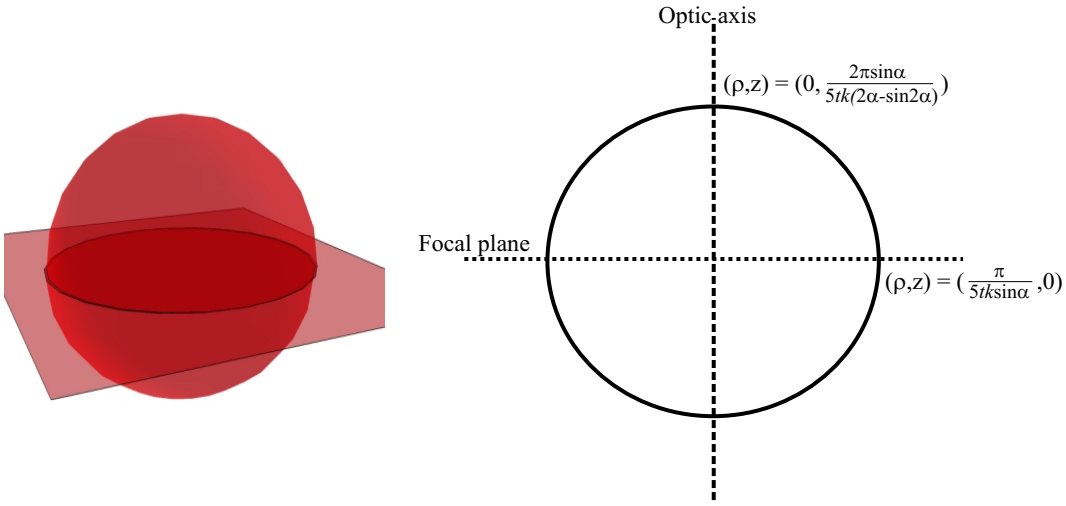

FIG. 6: The volume accessible to focal steering for the case where the adaptive element displays a wrapped phase shape and it is required that the focal intensity is at least 90% of that at the nominal focus.

IV. SAMPLING AND PIXELLATION EFFECTS OF THE SLM

The maximum phase gradient (or phase wrapping) is not the only factor to be taken into account when considering the focal positioning capabilities of the SLM. Additionally the influence of pixellation should be included [20], whereby the phase pattern on the SLM $\Psi(X, Y)$ is in fact sampled as an array of δ functions. The sampled array does not consist of infinitely narrow pixels and therefore the sampled phase should also be convolved with a "top-hat" function $\sqcap(X, Y)$. The pixellated version of $\Psi(X, Y)$ then becomes:

$$g_2(X, Y) = \left[\Psi(X, Y) \times \sum_{n_1, n_2} \delta(X - n_1 h, Y - n_2 h)\right] * \sqcap(X, Y) \tag{27}$$

with:

$$\sqcap(X,Y) = 1 \quad \text{for} \quad (-\frac{h}{2} < X \leq \frac{h}{2}) \quad \text{and} \quad (-\frac{h}{2} < Y \leq \frac{h}{2}) \tag{28}$$

$$= 0 \quad \text{otherwise} \tag{29}$$

where h represents the period of the pixel array and the summation is carried out over the SLM display area. When the the beam is transformed by a lens, the consequent field in the focal plane is proportional to the Fourier Transform of the pixellated phase:

$$G(x,y) = \mathcal{F}\{g_2(X,Y)\} \tag{30}$$

$$= \left[\psi(x,y) * \sum_{n_1,n_2} \delta(x - n_1\frac{\lambda f}{h}, y - n_2\frac{\lambda f}{h})\right] \text{sinc}(\frac{kh}{2f}x)\text{sinc}(\frac{kh}{2f}y) \tag{31}$$

where f is the focal length of the lens used and $\psi(x,y) = \mathcal{F}\{\Psi(X,Y)\}$. Thus the effect of sampling the phase $\Psi(X,Y)$ is that the field in the focal plane is repeated in an array of period $\frac{\lambda f}{h}$ and is subject to an amplitude apodisation $\text{sinc}(\frac{kh}{2f}x)\text{sinc}(\frac{kh}{2f}y)$ due to the finite pixel size.

V. EXPERIMENT

The experimental setup is shown in Figure 7. A continuous wave diode laser (Coherent Cube 785-40c) with wavelength $\lambda = 785$ nm was expanded onto a reflective phase-only liquid crystal SLM (X10468-02, Hamamatsu Photonics). The beam was subsequently focussed onto a CCD by an achromatic doublet with focal length 300 mm. The focal spot was steered within the plane of the CCD by applying a linear phase gradient across the SLM. The results are presented in Figure 7 (b) for the intensity of the focal spot, normalised to that at the nominal focus, as a function of position. The intensity is observed to drop off with increasing displacement as expected. A good analytic fit to the data can be readily achieved simply by considering the effects of phase wrapping (Equation 26 with $z = 0$) and pixellation (Equation 31):

$$\frac{I}{I_0} = \left(\pi - \frac{tk\rho}{2}\sin\alpha\right)\text{sinc}^2\left(\frac{kh\rho}{2f}\right) \tag{32}$$

A least squares fit to the data yields a value for the effective width of a phase wrap on the SLM as $t = 23.5$ μm. This is slightly larger than a single pixel on the SLM ($h = 20$ μm) and can be understood as an effect of the continuum nature of the liquid crystal medium and fringing electric fields at the pixel edge.

VI. CONCLUSION

An analytic model is developed to describe the capabilities of an AOE to steer a single focus within the focal region of a lens. We show how the distance to which a focus may be displaced is limited by the maximum phase gradient or modulation range achievable for a given AOE. Furthermore, as the focus is steered further from the natural focus using liquid crystal SLMs, the intensity is reduced due to the presence of wrapping in the required phase

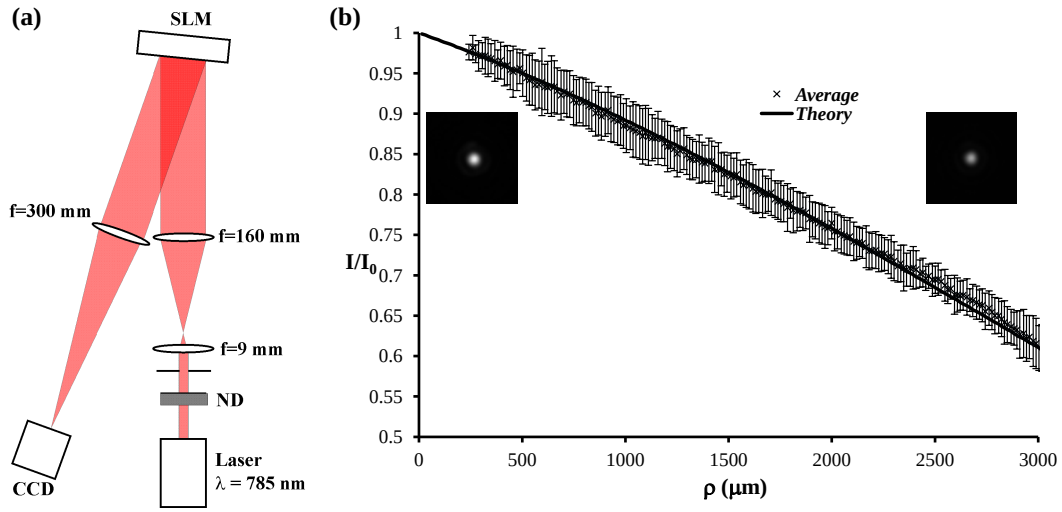

FIG. 7: (a) The experimental system. (b) The normalised focal intensity when using the SLM to steer the focus within the focal plane.

pattern. This reduction in intensity is accounted for in our model by assigning an effective width t to each phase wrap, and integrating over the SLM display to determine the area occupied by phase wrapping. We predict that as the focus is shifted in either the focal plane or along the optic axis there will be a linear decrease in focal intensity with respect to distance due to the phase wrapping. The efficiency of the beam steering is also directly proportional to the effective width of the phase wrap region. This linear term should be combined with an additional $\mathrm{sinc}^2(\ldots)$ modulation due to the SLM pixellation in order to fully describe the intensity reduction as a function of position. There is a good agreement between our model and experimental measurements of steering the focus within the focal plane, which allow us to characterise the effective width t for the flyback region of our SLM.

While we have dealt here with the case of steering a single focal spot within the focal volume, we note that the analysis presented is more generally useful. By integrating the desired phase pattern over the pupil, we do not limit ourself to the simple cases of applying tip, tilt and defocus, but are also able to cope with more complicated beam steering. This might include the case where any aberrations encountered as a result of the beam steering are simultaneously compensated, which is especially relevant for motion along the optic axis [13, 21, 22]. Additionally the analysis can be extended to the case where the phase pattern, or hologram, displayed on the spatial light modulator generates multiple focal spots, which is of interest in both optical trapping [5, 6, 23, 24] and laser fabrication [7, 8]. We are still able to determine the area of the pupil occupied by phase wraps, and use this to estimate the intensity of the zero order, which is found at the nominal focus and collects the majority of light that is not appropriately directed by the hologram. This is useful knowledge if the zero order is to be removed through destructive interference [8, 25]. Furthermore we can draw analogy from our analysis between the accessible volume for steering a single focus and the appropriate volume available for a multiple spot array.

Acknowledgments

This research was supported by funding from the Engineering and Physical Sciences Research Council, UK (grant numbers EP/H049037/1 and EP/E055818/1).

---

[1] P. F. McManamon, T. A. Dorschner, D. L. Corkum, L. J. Friedman, D. S. Hobbs, M. Holz, S. Liberman, H. Q. Nguyen, D. P. Resler, R. C. Sharp, et al., Proc. IEEE **84**, 268 (1996).
[2] G. D. Love, Appl. Opt. **36**, 1517 (1997).
[3] M. J. Booth, Phil. Trans. R. Soc. A **365**, 2829 (2007).
[4] A. Wiener, Rev. Sci. Instr. **71**, 1930 (2000).
[5] M. Reicherter, T. Haist, E. U. Wagemann, and H. J. Tiziani, Opt. Lett. **24**, 608 (1999).
[6] E. R. Dufresne, G. C. Spalding, M. T. Dearing, S. A. Sheets, and D. G. Grier, Rev. Sci. Instr. **72**, 1810 (2001).
[7] S. Hasegawa, Y. Hayasaki, and N. Nishida, Opt. Lett. **31**, 1705 (2006).
[8] A. Jesacher and M. J. Booth, Opt. Express **18**, 21090 (2010).
[9] D. P. Resler, D. S. Hobbs, R. C. Sharp, L. J. Friedman, and T. A. Dorschner, Opt. Lett. **21**, 689 (1996).
[10] I. G. Manolis, T. D. Wilkinson, M. M. Redmond, and W. A. Crossland, IEEE Photon. Technol. Lett. **14**, 801 (2002).
[11] A. J. Cable, E. Buckley, P. Marsh, N. Lawrence, T. D. Wilkinson, and W. A. Crossland, SID International Symposium Digest of Technical Papers **35**, 1431 (2004).
[12] R. Bowman, A. Jesacher, G. Thalhammer, G. Gibson, M. Ritsch-Marte, and M. Padgett, Opt. Express **19**, 9908 (2011).
[13] G. Sinclair, P. Jordan, J. Leach, and M. J. Padgett, Jnl. Mod. Opt. **51**, 409 (2004).
[14] E. Hallstig, J. Stigwall, T. Martin, L. Sjoqvist, and M. Lindgren, Jnl. Mod. Opt. **51**, 1233 (2004).
[15] X. Wang, B. Wang, P. J. Bos, J. E. Anderson, J. J. Pouch, and F. A. Miranda, J. Opt. Soc. Am. A **22**, 346 (2005).
[16] A. G. Georgiou, M. Komarcevic, T. D. Wilkinson, and W. A. Crossland, Mol. Cryst. Liq. Cryst. **434**, 183/[511] (2005).
[17] R. James, F. A. Fernndez, S. E. Day, M. Komarcevic, and W. A. Crossland, J. Opt. Soc. Am. A **24**, 2464 (2007).
[18] M. Gu, *Advanced Optical Imaging Theory* (Springer, 2000).
[19] M. Abramowitz and I. A. Stegun, *Handbook of mathematical functions* (Dover, 1970).
[20] V. Arrizon and M. Testorf, Opt. Lett. **22**, 197 (1997).
[21] M. J. Booth, M. A. A. Neil, and T. Wilson, Journal of Microscopy **192**, 90 (1998).
[22] T. Ota, S. Kawata, T. Sugiura, M. J. Booth, M. A. A. Neil, R. Juskaitis, and T. Wilson, Opt. Lett. **28**, 465 (2003).
[23] R. D. Leonardo, F. Ianni, and G. Ruocco, Opt. Express **15**, 1913 (2007).
[24] J. Leach, G. Sinclair, P. Jordan, M. J. Padgett, J. Courtial, J. Cooper, and Z. J. Laczik, Opt. Express **12**, 220 (2004).
[25] D. Palima and V. R. Daria, Appl. Opt. **46**, 4197 (2007).